Draft version January 8, 2026
Typeset using LaTeX **twocolumn** style in AASTeX7

Mutual Orbit Alignment in Resolved Triple Systems

Andrei Tokovinin[1]

[1] *Cerro Tololo Inter-American Observatory — NSF's NOIRLab Casilla 603, La Serena, Chile*

ABSTRACT

A sample of 278 triple systems with outer separations under 300 au and resolved inner pairs is studied, focusing on the mutual alignment between inner and outer orbits. The degree of alignment increases with (i) decreasing outer separation, (ii) decreasing ratio of outer and inner separations, (iii) decreasing mass of the inner primary component, and (iv) increasing inner mass ratio. There is no dependence on the outer mass ratio. The average mutual inclination is ∼40°for the full sample and ∼10°for 38 triples with primary components less massive than 1 $M_\odot$ and outer separations below 50 au. Inner eccentricities in aligned triples are smaller compared to misaligned ones. In another sample of 371 hierarchies with known outer orbits and inner eclipsing subsystems, only 22% show mutual alignment within 20°, while the rest are aligned randomly. These findings match qualitatively current understanding of the formation of hierarchical systems, where the N-body dynamics dominates at large scales, while the accretion and migration shape systems closer than ∼100 au. Fragmentation of isolated cores apparently produces approximately aligned low-mass hierarchies.

Keywords: binaries:visual — stars:multiple — stars:low-mass

1. INTRODUCTION

The genesis of binary stars and higher-order hierarchies is an important but still poorly understood aspect of star formation (S. S. R. Offner et al. 2023; A. Tokovinin 2021a). The solution of this problem is hindered by the lack of reliable statistics of high-order multiplicity caused by observational limitations such as angular resolution and spectroscopic coverage. On the other hand, the theory of multiple-star formation is still in its infancy: diverse physical processes play a substantial role, but their modeling and relative importance is a subject of ongoing effort. Joining the two ends, theory and observations, remains a challenge. In this contribution I address the issue of relative orbit alignment in triple stars using recent data. In a broader context, this work complements studies of relative inclinations between stellar rotation axes and orbits of binaries (M. L. Marcussen & S. H. Albrecht 2022) and planets (S. H. Albrecht et al. 2022), and of the alignment of planetary orbits within binaries (T. J. Dupuy et al. 2022; S. Christian et al. 2025).

The Gaia mission (Gaia Collaboration et al. 2016, 2021) makes fundamental contributions in many areas, including stellar multiplicity. The uniform astrometric and photometric coverage of the whole sky with well-defined detection limits identifies wide physical binaries and hierarchies, enabling unbiased evaluation of their statistics. The angular resolution of the current Gaia Data Release 3 (GDR3) is on the order of 1″, giving access to separations above ∼100 au at 100 pc distance. The catalog of ∼1 million wide pairs derived from GDR3 supersedes prior samples by orders of magnitude (K. El-Badry et al. 2021). Extension of this effort to triple stars identifies ∼10,000 wide hierarchies within 500 pc (C. Shariat et al. 2025). These authors extend the earlier study by A. Tokovinin (2022) based on a much smaller but cleaner sample of wide triples within 100 pc. Their statistics largely match the predictions of pure gravitational N-body dynamics, but indicate that at separations below 100 au the orbits become partially aligned. The components' masses in wide triples do not correspond to a random draw from the initial mass function (IMF): they are correlated and, on average, are larger compared to single field stars.

However, Gaia has a modest angular resolution and a limited time base. Many new close triples have been discovered during the last decade using ground-based methods, especially among low-mass stars (see section 2.1). This work uses the modern speckle data and updates the studies of relative orbit alignment by M. F. Sterzik & A. A. Tokovinin (2002) and A. Tokovinin (2017).

The mutual inclination Φ between the inner and outer orbits (i.e. the angle between their orbital angular momentum vectors) in a triple system can be computed from the known orbital elements. Aligned, orthogonal, and anti-aligned orbits correspond to $\Phi = 0$, $\Phi = \pi/2$, and $\Phi = \pi$, respectively. The elements of the inner and outer orbits with correct node identification are available only for a small sample. However, a powerful statistical measure of mutual alignment is the correlation between the observed sense of motion, i.e. the numbers of co- and counterrotating triples n_+ and n_- (C. E. Worley 1967; M. F. Sterzik & A. A. Tokovinin 2002). The sign correlation C is defined as

$$C = (n_+ - n_-)/(n_+ + n_-) = 1 - 2\langle\Phi\rangle/\pi. \quad (1)$$

If co- and counterrotating triples are assigned $S = 1$ and $S = -1$, respectively, the sign correlation is simply the average value of S. The relation between C and the average mutual inclination $\langle\Phi\rangle$ follows from simple geometric considerations. For randomly aligned orbits, $C = 0$ and $\langle\Phi\rangle = \pi/2$. This method does not require knowledge of two orbits and nodes, hence is applicable to a much larger sample. However, C has only a statistical meaning. All aligned systems corotate, but the inverse is not true: half of the randomly aligned systems also corotate, so the significance of S for individual triples is not high. The motion sense is poorly defined for orbits seen edge-on. Excluding such systems (as done here) gives more robust results, but the relation between C and $\langle\Phi\rangle$ becomes only approximate because the assumption of uniform orientation of orbits relative to the observer is no longer accurate.

Here I study resolved triple systems with outer separations below ∼300 au to explore the transition from misalignment at large separations to prevailing alignment of more compact hierarchies. The increased size of the modern sample allows us to probe the dependence of the mutual alignment on the separation and other parameters such as mass and mass ratio. Section 2 presents the observational data, the sample, and the determination of relative motions. Statistics of this sample are the subject of Section 3, where the additional samples of 2+2 resolved quadruples and triples with inner eclipsing subsystems are characterized. Section 4 compares findings of this study with theory and simulations.

2. DATA

2.1. *Observations*

In recent years, adaptive optics and speckle interferometry have opened a new window into the low-mass hierarchical systems among nearby stars. These objects are found during multiplicity surveys in the field (e.g. C. Leinert et al. 1997; M. Janson et al. 2014; J. G. Winters et al. 2019; C. A. Clark et al. 2024) and in young associations (A. Tokovinin & C. Briceño 2020). New hierarchies are also discovered serendipitously in high-resolution observations of known visual binaries, revealing one of their components as a tight pair. The growing number of known triples and higher-order systems is reflected in the Multiple Star Catalog (MSC) (A. Tokovinin 2018a). Its last (December 2023) public update available online[2] contains ∼4000 systems. Each hierarchy is identified by its MSC code based on the J2000 position, similar to (and, mostly, coincident with) such codes in the Washington Double Star Catalog (WDS) (B. D. Mason et al. 2001).

To determine relative motions and orbital configurations of resolved hierarchies, their discovery should be followed by monitoring during several years or decades. Such a long-term program is being conducted at the 4.1 m Southern Astrophysical Research (SOAR) telescope in Chile using speckle interferometry. The instrument and data reduction are covered in (A. Tokovinin et al. 2010; A. Tokovinin 2018b). The speckle measurements and resulting orbits are published in a series of papers (the latest is A. Tokovinin et al. 2024) and used for the study of individual resolved hierarchies (A. Tokovinin & D. W. Latham 2017; A. Tokovinin 2018c; A. Tokovinin & D. W. Latham 2020; A. Tokovinin 2021a, 2023a, 2025a,b). These data are incorporated in the present work.

To illustrate the speckle monitoring at SOAR, Figure 1 plots the data for 00247−2653 (LHS 1070). This remarkable triple system bordering the stellar and substellar regimes (masses of 0.15, 0.07, 0.07 $M_\odot$) has been discovered by C. Leinert et al. (1997) in 1993.6. Owing to the strong interaction between the inner and outer subsystems, the approximation of motion by two Keplerian orbits is rather crude (F. Xia et al. 2019). Nevertheless, the two-orbit fit to the data up to 2025.5 yields the inner and outer periods of 17.26±0.01 and 83.06±1.71 years, respectively, and the eccentricities of $e_{\rm in} = 0.0170 \pm 0.0008$ and $e_{\rm out} = 0.036 \pm 0.007$. The mutual inclination is 2.°0±0.°4, and the period ratio is 4.81±0.10, near the limit of the dynamical stability and suggestive of a 1:5 mean motion resonance. Although three decades of monitoring cover only a fraction of the outer orbit, its character is already well constrained. The low-mass (M4.5V) triple 10367+1522 (DAE 3) has a similar architecture with periods of 8.6 and 120 yr, small eccentricities, and aligned orbits. Another inter-

[2] http://vizier.u-strasbg.fr/viz-bin/VizieR-4?-source=J/ApJS/235/6 and https://www.ctio.noirlab.edu/~atokovin/stars/

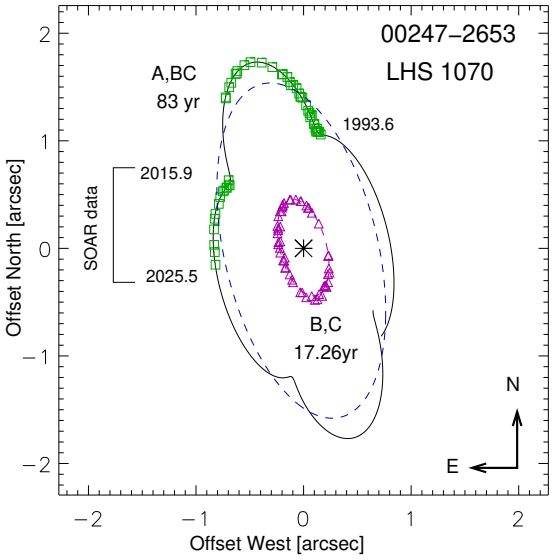

Figure 1. Observed orbital motions in the low-mass triple system 00247−2653 (LHS 1070) are approximated by two Keplerian orbits, highlighting the decade of monitoring at SOAR. The positions of the inner pair B,C are plotted by magenta triangles, and the positions of A,B by green squares. The solid line shows the outer orbit with wobble, the dashed line is the outer orbit of the center of mass BC around A.

esting triple system DENIS J020529.0−115925 consisting of three brown dwarfs (H. Bouy et al. 2005) with an outer separation of 8 au still lacks data on its orbital motion.

The detailed view of the orbital dynamics illustrated above is possible only for a few well-studied triples. For the recently discovered systems, the available measurements cover only small orbital arcs, especially in the slowly moving outer pairs.

2.2. *Sample*

The sample of resolved hierarchies is based on the current version of the MSC. This is a heterogeneous collection of observations, incomplete even within the 100 pc volume (A. Tokovinin 2023b). The observational limits in resolution and contrast leave a strong imprint on the statistics of separations and mass ratios of those systems. However, these limitations should not affect the observed *relative motions*. This study focuses on the analysis of orbital motions, recognizing that other parameters in this sample are selection-dependent.

Masses in the MSC are derived from the absolute magnitudes using standard relations for dwarfs (M. J. Pecaut & E. E. Mamajek 2013). The period P^* is estimated from the projected separation (its median is close to the semimajor axis), unless the true period P is known. The statistical relation between projected separation and semimajor axis is covered in several papers, e.g. in the Appendix of A. Tokovinin et al. (2020) and in V. V. Makarov (2025). In this, study I select hierarchies with outer periods shorter than 10^6 days (2.7 kyr), which corresponds to separations below ∼300 au. This cut is imposed because wider hierarchies in the field are already well characterized by Gaia, and here I want to explore in greater detail the transition from random orbit orientation to alignment.

To allow determination of the inner orbit orientation, the inner subsystem should have a known astrometric or visual orbit or, at least, be directly resolved. I eliminate a few resolved inner subsystems with periods shorter than 100 days and resolved triples where the inner pair contains an even closer (e.g. eclipsing) subsystems, but retain hierarchies where the resolved triple has wider companion(s). The reason is to study only triples within limited range of inner and outer periods. The resolved quadruples of 2+2 type (two close pairs) are also excluded from this sample and discussed separately in section 3.4, while section 3.5 explores the alignment of inner eclipsing pairs in triples with resolved outer components.

The original selection of 355 candidates from the MSC is reduced to 278 systems where the orbits or the directions of relative motion could be determined in both outer and inner pairs. Table 1 in section 2.4 lists these hierarchies and their main parameters. The inner and outer orbits are known in 176 and 76 triples, respectively. Although some orbits are tentative or preliminary (especially with long periods), the motion direction is defined reliably. The remaining 102 inner and 202 outer subsystems have known direction of relative motion, discussed in the following section.

The present sample partially overlaps with my earlier study (A. Tokovinin 2017), but differs in several ways. The previous work did not restrict the outer periods and included both the 2+2 quadruples (considered as two triples) and the resolved triples with additional inner subsystems. The restrictions imposed here became feasible owing to the growing content of the MSC. Most objects in this sample are relatively recent discoveries from high-resolution imaging surveys of low-mass stars; the new sample includes triples without known inner orbits not considered in the earlier study.

2.3. *Relative Motions*

In this study, the published measurements retrieved from the WDS database (B. D. Mason et al. 2001) are combined with the SOAR data. The median parallax is 15 mas, so for half of the sample the outer separation of 300 au corresponds to an angular separation of $>4\farcs5$, and GDR3 can contain astrometric solutions for both sources. However, the proper motions of unresolved in-

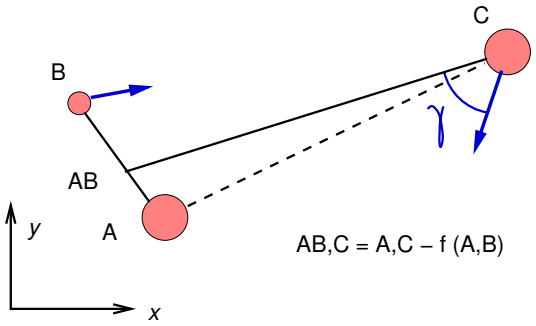

Figure 2. Relative motions in a triple system of hierarchy AB–C (section 2.3). AB is the center of mass of the inner subsystem A,B. Blue arrows indicate the motion directions. The angle between the radius-vector joing the components and the motion direction is γ.

ner pairs are biased by their orbital motions (except those with Gaia astrometric orbits) and, lacking good models of these motions for the mean epoch of 2016.0, I cannot compute and subtract this bias to isolate the motion of the outer pair, as has been done for resolved Gaia triples (A. Tokovinin 2022). Here I rely only on the relative positions and orbits.

The relative astrometry of resolved triples refers to the individual stars: positions of the secondary component B relative to the primary A in the inner subsystem and of the tertiary star C relative to A. The positions are measured as a function of time, as illustrated in Figure 2. The polar coordinates (ρ, θ) are converted into Cartesian coordinates x, y, where x points to the north and y to the east. The observed trajectories are approximated by linear functions of time, e.g.

$$x(t) = \rho(t)\cos\theta(t) \approx x_0 + \dot{x}(t - t_0), \qquad (2)$$

where t_0 is the mean time of observations. The position vector at t_0 is (x_0, y_0), and the relative speed vector is $(\dot{x}, \dot{y})$. The angle γ between these vectors contains information on the direction of the relative motion (it is counterclockwise, also called direct, for $0 < \gamma < 180°$) and is statistically related to the distribution of eccentricities (A. Tokovinin & O. Kiyaeva 2016).

The motion of the outer pair should be in reference to the center of mass of the inner subsystem, denoted as AB. To do so, the measured relative positions of A,C are corrected by adding the positions of A,B scaled by the wobble factor $|f| = q_{\rm in}/(1+q_{\rm in})$, depending on the inner mass ratio $q_{\rm in} = m_B/m_A$. This factor is negative when the subsystem belongs to the primary, as shown in Figure 2, and positive when it is in the secondary (A–BC hierarchy). When the inner orbit is known, the positions are computed from its elements; otherwise, from the linear model (2). If the outer arc is measured during several inner periods, the inner motion does not affect the linear fit of the outer pair.

Figure 3 illustrates three low-mass triples from this sample. The first one, 02490−1029, was discovered in 2008 by M. Janson et al. (2014). Currently its configuration is non-hierarchical, with the inner and outer separations of 0.″19 and 0.″58, respectively. Both pairs move counterclockwise. The second triple 04007−2305 (GJ 3260) has been discovered at SOAR in 2016; its subsystems move clockwise. In both triples the observed arcs are much larger than the measurement errors, allowing reliable determination of the relative speed. The third example illustrates the triple 06460−6624 (discovered at SOAR in 2019) with counterrotating subsystems and known inner orbit.

Approximation of the observed arcs by linear functions of time is quite crude, but sufficient for the purpose of this study. To simplify, no weights are used in the linear fits when combining measurements from different sources. The errors of the speed components $\dot{x}$ and $\dot{y}$ are determined from these fits if three or more measurements are available; for two measurements, the unknown errors are set to zero. The speed of the relative motion $\mu = \sqrt{\dot{x}^2 + \dot{y}^2}$ can be normalized by the nominal speed, $\mu' = \mu/\mu^*$ (A. Tokovinin & O. Kiyaeva 2016), where

$$\mu^* = 2\pi\varpi^{1.5}\rho^{-0.5}M^{0.5}. \qquad (3)$$

In this formula, $\rho = \sqrt{x_0^2 + y_0^2}$ is the angular separation, ϖ is the parallax, and M is the mass sum in solar units. The parameter μ^* corresponds to the speed in a circular face-on orbit with semimajor axis ρ. For bound pairs, $\mu' < \sqrt{2}$ (all outer pairs in this sample have $\mu' < 1.5$). The parameters μ' and γ are computed from the fitted linear models. The error of γ is estimated approximately as $\sigma_\gamma \approx 57.^\circ3\ \sigma_\mu/\mu$, assuming equal speed errors in the radial and tangential directions.

In addition to the linear models, the observed motion can be characterized by the areal constant $A_z = 0.5\rho^2\dot{\theta}$ determined from the observations. It is proportional to the projection of the total angular momentum of the orbit on the line of sight. The full areal constant A (area of the orbital ellipse divided by the period) is related to the semimajor axis a (in angular units), period P, and eccentricity e as

$$A = \pi a^2\sqrt{1-e^2}/P = \pi\sqrt{1-e^2}a^{0.5}\varpi^{1.5}M^{-0.5}, \qquad (4)$$

where the last expression is obtained from the third Kepler law. Obviously, $A_z = A\cos i$. If the semimajor axis a were known, the ratio A_z/A would inform us on the orbital inclination i. For crude estimates, the factor

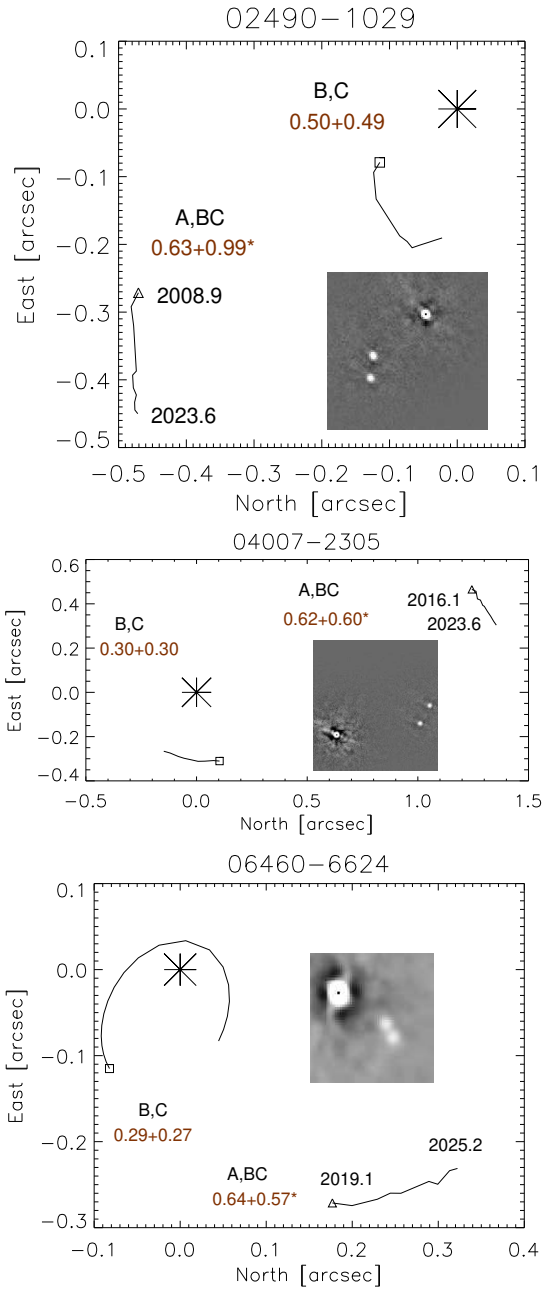

Figure 3. Observed relative motions in three selected low–mass triples. The coordinate origin is marked by a large asterisk. Relative positions of the inner and outer pairs are plotted by solid lines, with the times of the first and last observations indicated. The brown numbers are component's masses. The outer positions refer to the center of mass of the inner pair. The first positions of the inner and outer pairs are marked by the square and triangle, respectively. The inserts show the speckle images of these triples from the latest observations at SOAR. In 06460−6624, the observed part of the 11.7 yr inner orbit of B,C is plotted; note the opposite motion sense of the inner and outer pairs in this triple.

$\sqrt{1-e^2}$ can be neglected (it is above 0.87 for $e < 0.5$), and a can be replaced by the observed separation ρ. For the triple 02490−1029 shown in Figure 3, the inner pair has $A_z/A = 0.88$ — a strong indication of a face-on orbit. For the outer pair, $A_z/A = 1.9$, which means that the current separation ρ is less than the true semimajor axis a, thus underestimating A. So, the apparently non-hierarchical configuration of this triple is a result of projection. For the counterrotating triple 06460−6624, $A_z/A = 1.4$, also indicating that a is larger than ρ in the outer orbit. In these "trapezia" triples, the outer periods P^* are underestimated because the projected separations happen to be smaller than the true semimajor axes.

We can invert the relation (4) to estimate the lower limit of the semimajor axis a in angular units from the measured parameter A_z, without using the separation:

$$a = \frac{A_z^2 M}{\pi^2 \varpi^3 (1-e^2)\cos^2 i} > A_z^2 M \pi^{-2} \varpi^{-3} = a_{\min}. \quad (5)$$

For random orbit orientation, $\cos i$ is distributed uniformly, the median of $\cos^2 i$ is 0.25, and $a > 4a_{\min}$ is a better statistical estimate. For the apparently non-hierarchical configurations of 02490−1029 and 06460−6624, the $4a_{\min}$ axes of the outer orbits are 7.″8 and 2.″3, respectively, much larger than their current outer separations of 0.″6 and 0.″4.

2.4. *Data tables*

Examples of the tables are described here, and the full tables are available as data files. Table 1 lists global parameters of the hierarchical systems in our sample. The first column gives the MSC code based on the J2000 position; it can be used to access complementary information contained in the MSC. The masses of the inner pair m_1 and m_2 and of the tertiary component m_3 are given in the next three columns, followed by the parallax ϖ. Then the decimal logarithm of the period in days and the semimajor axis or projected separation in au are given for the inner and outer subsystems. The solution types indicate whether an orbit (2) or only a linear model (1) are available. The sign correlation S takes values of +1 and −1 for corotating and counterrotating triples, respectively, and zero for systems excluded from the statistics for the reasons given in section 3.3. The last column contains the separation of the outer (fourth) companion in au, if present.

The orbital elements used in this study are listed in Table 2. Each pair is identified by the MSC code and a tag I (inner) or O (outer). The 7 elements are provided in standard notation (P — orbital period, T — epoch of periastron, e — eccentricity, a — semimajor axis,

Table 1. Sample Summary (Fragment)

MSC	m_1	m_2	m_3	ϖ	log $P_{\rm in}$	$a_{\rm in}$	log $P_{\rm out}$	$a_{\rm out}$	Solution		S	$a_{\rm ext}$
(J2000)		($M_\odot$)		(mas)	(d)	(au)	(d)	(au)	In	Out		(au)
00164−2235	1.40	0.99	0.72	9.84	4.02	12.6	5.39	111.8	2	1	1	0
00174+0853	1.28	1.13	1.26	14.47	4.11	14.5	5.93	272.6	2	1	0	0
00247−2653	0.08	0.08	0.11	129.30	3.80	3.7	4.48	12.4	2	2	1	0
00304−6236	0.54	0.49	0.23	22.34	4.05	9.9	5.96	198.1	2	1	0	0
00325+6714	0.41	0.16	0.31	101.09	3.75	5.1	4.91	35.1	2	2	1	0
00329−0434	0.21	0.10	0.12	52.85	3.72	4.0	4.65	18.5	2	1	0	0
01158−6853	1.38	0.30	0.88	47.65	3.47	4.8	5.64	154.5	2	2	1	6692

Table 2. Orbital Elements (Fragment)

MSC	In/Out	P	T	e	a	Ω	ω	i	Reference[a]
(J2000)		(yr)	(yr)		($''$)	(deg)	(deg)	(deg)	
00164−2235	I	28.834	2000.281	0.674	0.144	61.1	38.9	137.5	Tok2023a
00174+0853	I	35.660	1950.700	0.002	0.189	124.1	282.0	95.4	Hrt2010a
00247−2653	I	17.260	2006.445	0.017	0.460	14.9	202.5	62.1	New
00247−2653	O	83.060	2070.117	0.036	1.592	13.2	285.2	63.3	New
00304−6236	I	30.000	2016.880	0.430	0.202	95.8	41.1	132.2	New

[a] Orbit references are provided at https://crf.usno.navy.mil/data_products/WDS/orb6/wdsref.html and in the data file.

Table 3. Linear Elements (Fragment)

MSC	In/Out	t_0	x_0	y_0	$\dot{x}$	$\dot{y}$	$\sigma_{\dot{x}}$	$\sigma_{\dot{y}}$	γ	σ_γ
(J2000)		(yr)	($''$)	($''$)	(mas yr^{-1})		(mas yr^{-1})		(deg)	(deg)
00164−2235	O	2020.17	−0.244	−0.997	−7.4	3.2	0.4	0.9	260.0	7.0
00174+0853	O	1933.79	−2.464	−3.510	1.4	5.1	0.4	0.8	199.7	9.3
00304−6236	O	2006.19	−2.219	−3.703	−8.9	−14.3	3.1	1.0	359.0	11.0
00329−0434	O	2022.56	−0.927	−0.243	−31.4	−16.8	2.5	1.3	13.5	4.5
00541+6626	O	2010.19	−0.295	0.828	4.4	2.5	0.5	0.4	279.5	7.3
01036−5516	O	2009.48	1.566	−0.752	1.4	−7.9	2.2	5.1	305.9	39.4

Ω — position angle of ascending node, ω — longitude of periastron, i — inclination). The last column gives reference codes to these orbits borrowed from the 6th orbit catalog (W. I. Hartkopf et al. 2001) and complemented where necessary; "New" indicates unpublished orbits computed or modified by the author.

Table 3 lists linear models for pairs without known orbits. Its first two columns are same as in Table 2. Then follow the mean time t_0, coordinates x_0 and y_0 at this time, the velocity components $\dot{x}$ and $\dot{y}$, their formal errors, the angle γ, and its error.

3. STATISTICS

3.1. *Periods and Masses*

Figure 4, top, plots the inner and outer periods in this sample (red squares and asterisks) in comparison with other known hierarchies (pale plus crosses). The combination of the imposed period cuts and the requirement to resolve the inner subsystem in our sample results in clustering of the points above the dynamical stability limit $P_{\rm out}/P_{\rm in} > 4.7$ (R. A. Mardling & S. J. Aarseth 2001). Points below this line have underestimated outer periods owing to projection, as explained above in section 2.3.

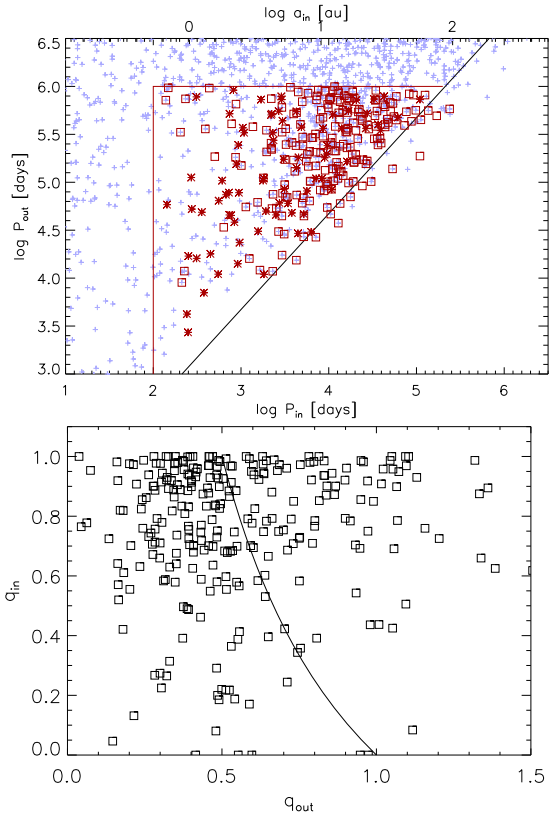

Figure 4. Top: periods of the inner and outer subsystems in multiple stars. Small blue crosses denote hierarchies within 200 pc with primary masses less than 1.5 $M_\odot$. Large red symbols mark our sample of triples with (asterisks) or without (squares) known orbits. The thin red line denotes the imposed limits on periods, and the thick solid diagonal line plots the nominal dynamical stability criterion $P_{\rm out}/P_{\rm in} > 4.7$ (R. A. Mardling & S. J. Aarseth 2001). Bottom: comparison between mass ratios in the inner and outer subsystems of our sample (squares). In 106 triples located to the right of the line, the tertiary is the most massive star.

The median masses of the inner primary and secondary components m_1 and m_2 are 0.88 and 0.70 $M_\odot$, respectively, and the median mass of the tertiary components m_3 is 0.80 $M_\odot$; in 106 triples the tertiary is the most massive star. Figure 4 (bottom) plots the inner mass ratio $q_{\rm in} = m_2/m_1$ vs. outer mass ratio $q_{\rm out} = m_3/(m_1 + m_2)$. The preference of large $q_{\rm in}$ could be a selection effect (pairs with small mass ratios escape detection in the imaging surveys), although it agrees with the simulations by P. F. Rohde et al. (2021) discussed below in section 4.1. The apparent concentration of points near $(0.5, 1)$ corresponds to three stars of comparable masses (triplets), and points near (1,1) are double twins with the inner and outer mass ratios close to one (the triple shown in Figure 1 is a double twin).

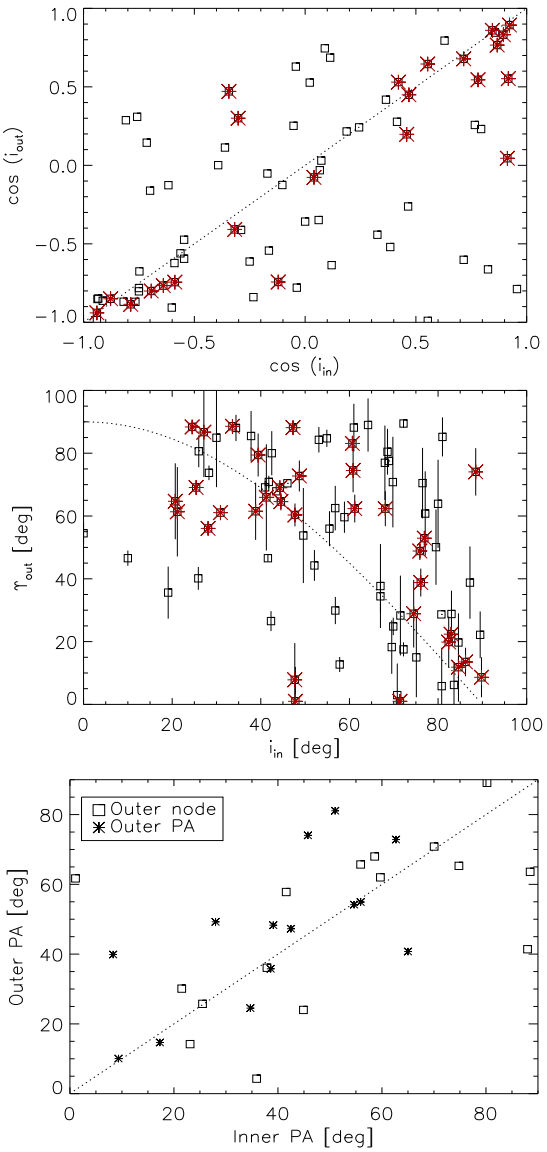

Figure 5. Top: comparison of the cosines of inner and outer orbital inclinations for 76 triples where both orbits are known. Middle: the angle γ in the outer pair vs. inclination of the inner orbit for 85 triples; the dotted line is $90^\circ \cos i_{\rm in}$. In both plots, red asterisks mark systems with inner primary mass below 0.8 $M_\odot$. Bottom: position angle of the outer pair vs. position angle of the inner pair for edge-on inner orbits; both angles are folded in the $(0, 90^\circ)$ interval. Squares and asterisks plot the nodal angles of 16 pairs with known outer orbits and the position angles of 14 outer companions with linear models, respectively.

3.2. *Orbital Inclinations*

The most complete information on the motion is available for the 76 triples where both inner and outer orbits are known. The relative angle Φ between the orbital

angular momentum vectors is computed as

$$\cos\Phi = \cos i_{\rm in}\cos i_{\rm out} + \sin i_{\rm in}\sin i_{\rm out}\cos(\Omega_{\rm in} - \Omega_{\rm out}), \quad (6)$$

where i are the inclinations and Ω the position angles of ascending nodes. However, the true ascending nodes are not known for most of these triples, so each pair of orbits gives two possible values of Φ corresponding to a 180° difference in $\Omega_{\rm in} - \Omega_{\rm out}$. For example, if both orbits are seen edge-on and their orientation on the sky is equal, Φ can be either 0 or 180°, and we cannot distinguish between the aligned and counteraligned cases. To circumvent the problem, two alternative values of Φ are computed for each triple with known orbits. The joint distribution of these angles indicates partial alignment, in agreement with my previous result (Figure 4 in A. Tokovinin 2017).

The similarity between orbital inclinations is a necessary (but not sufficient) condition for aligned orbits. Figure 5 (top) compares the cosines of inclinations for triples with two known orbits; it indicates prevailing alignment, with a few outliers. For example, 20396+0458 (HIP 101955) is a triple with reliably known and non-coplanar ($\Phi = 64\overset{\circ}{.}8 \pm 1\overset{\circ}{.}4$) orbits (A. Tokovinin & D. W. Latham 2017); its inner orbit has a substantial eccentricity of $e = 0.617$. The correlation coefficient between the cosines is 0.60±0.09 (its error is evaluated by bootstrap). If the sample is split into 23 systems with inner primaries less massive than 0.8 $M_\odot$ and 53 more massive triples, the correlation coefficients between the inclination cosines are 0.88±0.05 and 0.44±0.13, respectively. This indicates a stronger orbit alignment at lower mass.

The middle panel of Figure 5 compares the inclination of the inner orbit with the angle γ' in the outer pair for 85 triples with such data and $\sigma_\gamma < 20°$. The angles $\gamma' = \arcsin(|\sin\gamma|)$ and the inclinations are folded into the $(0, 90°)$ interval. If the orbits are aligned, radial motions are expected for the highly inclined orbits with $i_{\rm in}$ near 90°. Indeed, such a trend is seen, despite several outliers.

Finally, the lower plot in Figure 5 compares the position angles on the sky for 30 systems with approximately edge-on inner orbits ($i_{\rm in}$ from 80°to 100°). For 16 systems with both orbits known, the position angles of the ascending nodes Ω are folded in the $(0, 90°)$ interval as indicated above. For the additional 14 triples without known outer orbits, the folded position angles of the outer companions are plotted instead. The correlation between the angles is notable (correlation coefficient 0.58±0.13), suggesting some alignment between the subsystems. This plot uses only the position angles, and it can be produced for a larger sample with edge-on inner orbits where motions of the outer companions are not measured yet and only their position angles are known.

The qualitative results of this section complement the analysis of the sign correlation below from which the triples with highly inclined orbits and/or radial motions are excluded.

3.3. *Sign Correlation*

The motion direction is known when either orbits or linear fits are available. To reduce the impact of errors, I exclude the edge-on orbits with inclinations between 85° and 95° because without complementary data on radial velocities we cannot distinguish between co- and counterrotating cases. For subsystems without computed orbits, the motion direction is defined by the angle γ. Accounting for the measurement errors, the linear models with $0+2\sigma_\gamma < \gamma < 180-2\sigma_\gamma$ have direct motion, while for $180 + 2\sigma_\gamma < \gamma < 360 - 2\sigma_\gamma$ the motion is retrograde. Filtering out the edge-on orbits, noisy linear solutions with $\sigma_\gamma > 20°$, linear models with unknown σ_γ, and γ directions that are close to radial within $2\sigma_\gamma$ leaves 160 triples for the study of the sign correlation, where $S = +1$ stands for corotation and $S = -1$ for opposite rotation. The remaining triples have $S = 0$ in Table 1. The filtering leaves only 57% of the original sample; however, the data for the full sample are provided, and a less restrictive analysis of the sign correlation can be done by others.

Figure 6 plots $C = \langle S\rangle$ vs. several parameters: the outer separation, the separation ratio, the inner primary mass, the inner and outer mass ratios, and the inner eccentricity. To avoid overlap, the points are randomly displaced vertically from ±1. To quantify the trends, the sample is split into four equal groups over each parameter, and the sign correlation C in each group is plotted by squares and lines vs. average parameter in the group. The errors are computed from the binomial distribution, $\sigma_C = \sqrt{(1+C)(1-C)/N}$, where $N = 40$ is the group size.

The dependence of orbit alignment on the outer separation and on the separation ratio, noted earlier (M. F. Sterzik & A. A. Tokovinin 2002), is confirmed, as well as the trend of decreasing alignment with increasing mass. These trends are not totally independent owing to correlations between parameters; for example, low-mass triples tend to have larger mass ratios. The dependence of the degree of alignment on the inner mass ratio is a new result. On the other hand, there is no trend vs. outer mass ratio $q_{\rm out}$. Figure 6f plots the sign correlation vs. $e_{\rm in}$ for 125 triples with known inner orbits and known outer motion direction.

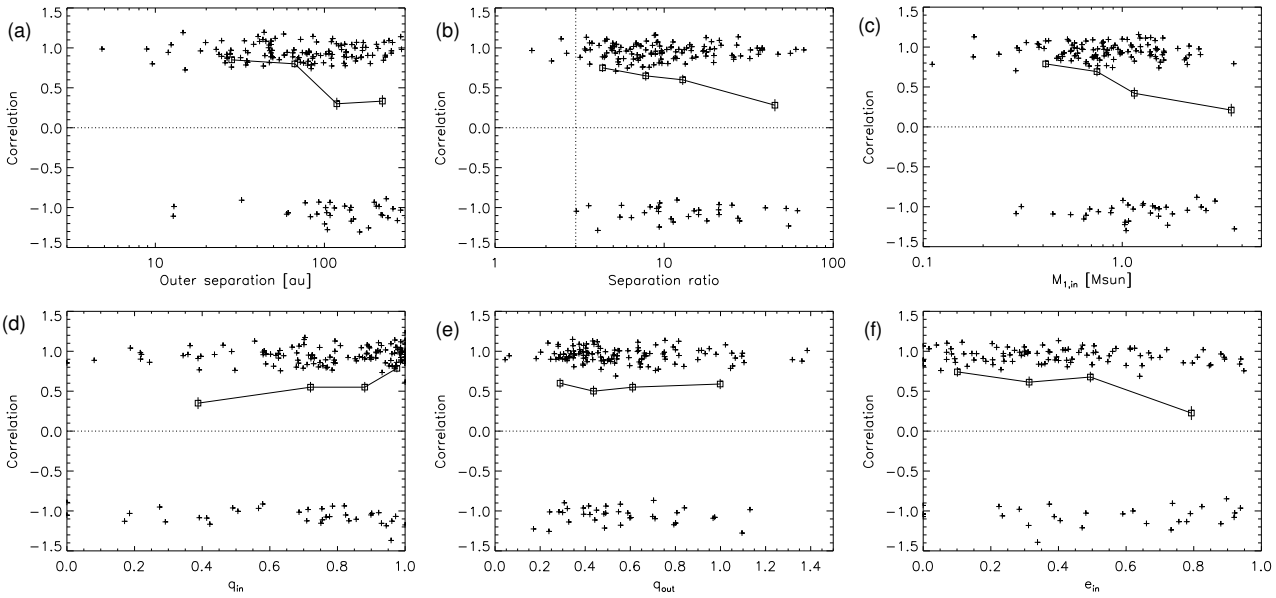

Figure 6. Relative motion direction S vs. several parameters: (a) outer separation, (b) separation ratio, (c) inner primary mass, (d) inner mass ratio, (e) outer mass ratio, and (f) inner eccentricity. The points are randomly displaced vertically to reduce overlap. The sample is split by each parameter into four equal groups. The squares with error bars and the thick lines plot the average sign correlation vs. average parameter value in each group.

Inner orbits in corotating triples are, on average, less eccentric (A. Tokovinin 2017). In the 98 triples with known inner orbits and $S = 1$, the median inner eccentricity is 0.37, while in the 27 counterrotating triples with $S = -1$ it is 0.58. The actual difference between eccentricities is larger because S has little meaning for individual systems, and among the 98 systems with $S = 1$ there are misaligned ones. However, statistically, the link between inner eccentricity and alignment is established reliably (Figure 6f). Both inner and outer orbits in the aligned low-mass triple system LHS1070 (Figure 1) are quasi-circular. Although the trend is clear, there are notable exceptions. In our sample, there are 30 inner orbits with eccentricity above 0.7, 24 of which have known relative motion. The sign correlation in this subset is low, 0.08±0.24.

For the full sample, $C = 0.56 \pm 0.10$ corresponds to the mean mutual inclination $\langle\Phi\rangle$ of 40° (this estimate is approximate). For the 65 triples with inner primaries below 0.8 $M_\odot$, $C = 0.75 \pm 0.16$, while for the remaining 95 more massive systems $C = 0.43 \pm 0.12$ ($\langle\Phi\rangle$ of 23° and 59°, respectively). The subsample of 38 triples with inner primaries below 1 $M_\odot$ and outer separations below 50 au has the largest degree of orbit alignment, $C = 0.89 \pm 0.22$ or $\langle\Phi\rangle \approx 10°$.

The general trends outlined here are not absolute, and hierarchical systems contradicting them are found infrequently but consistently, like the counterrotating low-mass double twin in the lower panel of Figure 3, or aligned low-mass triples with large inner eccentricities. For example, in the triple system 11247−6139 (HIP 55691) with a 0.74 $M_\odot$ inner primary, the measured mutual inclination between the 141 yr outer and 2.4 yr inner orbits is $6\overset{\circ}{.}5 \pm 0\overset{\circ}{.}8$. Yet, the inner eccentricity is 0.8802±0.0003 (A. Tokovinin 2025b). Another example is 08447−2126 (HIP 42910) with an inner eccentricity of 0.948±0.006 and apparently aligned orbits (A. Tokovinin 2023a).

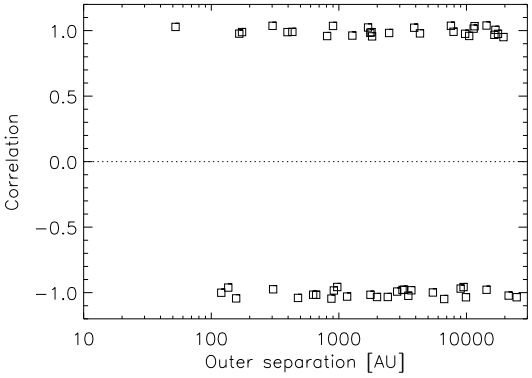

Figure 7. Relative motion directions of two inner pairs in 2+2 quadruples vs. outer separation.

3.4. *Resolved Quadruple Systems*

Quadruple systems of 2+2 hierarchy where both inner pairs are resolved are not included in the main sample. However, it is instructive to take a look at mutual orientations of inner orbits in these systems. Their list based on the MSC was examined manually to identify cases

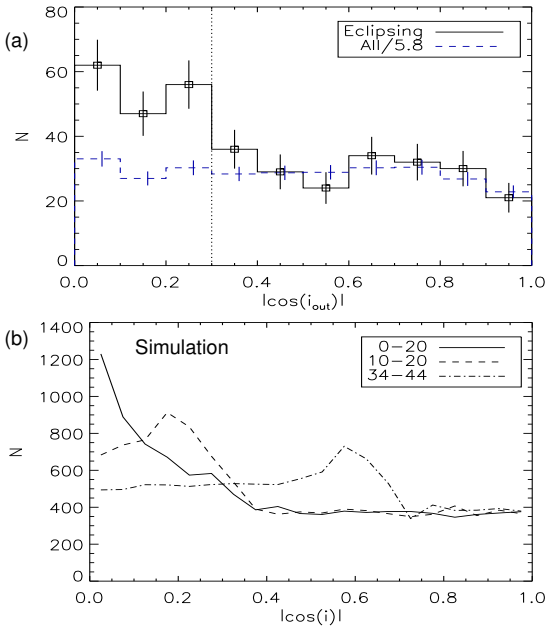

Figure 8. The histogram of $|\cos i_{\rm out}|$ in visual or astrometric binaries containing eclipsing subsystems is plotted in panel (a) by full line and squares with error bars, and the down-scaled histogram for all known orbital inclinations is plotted by the blue dashed line. Panel (b) shows histograms for simulated samples of triples where 0.75 fraction are aligned randomly, and the rest have mutual inclinations distributed in three intervals: full line — (0,20), dashed line — (10,20), and dash-dot line — (34,44) degrees.

where the direction of motion in both inner subsystems can be determined either from their orbits or, otherwise, from the position angle variation vs. time (without fitting linear models). In 63 such systems the mean sign correlation is $C = -0.14 \pm 0.12$. However, as shown in Figure 7, the outer separations in these quadruples are larger than in triples, with a median of 2.9 kau and only one below 100 au. So, the lack of mutual alignment between inner orbits in wide 2+2 quadruples agrees with the statistics of wide triples. Some hierarchies in this 2+2 sample contain additional subsystems, i.e. more than four components. As the 2+2 sample is only illustrative, it is not tabulated here.

Misalignment in several relatively compact (outer periods <500 yr) 2+2 quadruples where inner spectroscopic subsystems were resolved interferometrically is a rule rather than exception, for example in 04357+1010 (88 Tau, B. F. Lane et al. 2007), 07346+3153 (Castor, G. Torres et al. 2022), and 11221−2447 (HD 98800, S. Zúñiga-Fernández et al. 2021). A misaligned disk is found around one of the inner pairs in HD 98800.

Table 4. Alignment in the VA+E Sample

Sample	N	$N_{\rm align}$	f_a
All	371	80.4	0.217±0.040
$P_{\rm out} < 1000$ d	258	72.2	0.280±0.049
$P_{\rm out} > 1000$ d	113	8.2	0.073±0.068
$e_{\rm out} < 0.4$	203	54.6	0.269±0.055
$e_{\rm out} > 0.4$	168	25.8	0.154±0.057
$P_{\rm in} < 1$d	197	38.8	0.197±0.054
$P_{\rm in} > 1$d	174	41.6	0.239±0.058

3.5. *Eclipsing Subsystems in Visual and Astrometric Pairs*

To complement the study of resolved triples, I explore the distribution of known orbital inclinations in pairs containing inner eclipsing subsystems. Preliminary results of this study were presented at a conference (A. Tokovinin 2025c). As a first step, a sample of 1657 subsystems with known visual or astrometric orbits is extracted from the MSC. Most of them are relatively nearby (median parallax 11.7 mas). A subset of this sample containing 371 inner eclipsing binaries is defined. The majority of these triples are recent discoveries resulting from matching catalogs of eclipsing binaries with the Gaia catalog of astrometric orbits (D. R. Czavalinga et al. 2023); their outer periods are mostly shorter than 1000 days (the time span of the GDR3 mission). On average, triples containing eclipsing pairs (called VA+E for brevity) are more distant, their median parallax is 2.3 mas. The median masses in the full orbital sample and in its VA+E subset are 1.19 and 1.37 $M_\odot$, respectively.

The inclination of eclipsing subsystems should be close to 90°, and if they are aligned, a preference of edge-on outer orbits is expected. For orbits oriented randomly with respect to the observer, the cosine of inclination is distributed uniformly in $[-1, 1]$. Any alignment should be manifested by an excess of edge-on outer orbits with $|\cos i_{\rm out}| \sim 0$. The histogram of this quantity is shown in the upper panel of Figure 8. The distribution for the full sample with orbits (blue dashed line) appears almost uniform, but in the VA+E subsample there is an excess between 0 and 0.3.

To quantify the degree of alignment, I use the numbers N_1 and N_2 of the VA+E systems with $|\cos i_{\rm out}|$ below 0.3 and above 0.5, respectively. Then $N_{\rm align} = N_1 - (3/5)N_2$ is the excess of aligned systems relative to the uniform distribution. The fraction of this excess in the full sample N is $f_a = N_{\rm align}/N$. Its error is estimated approximately by the Poisson law,

$\sigma_f = \sqrt{N_1 + 0.6^2 N_2}/N$. Table 4 lists these parameters for the full sample and its cuts.

The first conclusion is that about 78% of hierarchies in the VA+E sample do not show any alignment between their inner and outer orbits, while the remaining 22±4% are aligned within $|\cos i_{\rm out}| < 0.3$ ($i_{\rm out}$ of 90°±17°.5). The excess of aligned subsystems is statistically significant at the 5.4σ level. Note that the orbits of eclipsing binaries may have inclinations different from 90°, while the inclinations of visual and astrometric orbits are affected by the measurement errors. These effects broaden the observed distribution, so its width is an upper limit of the true mutual alignment.

The fraction of aligned hierarchies in the VA+E sample apparently depends on the outer period, being larger for compact triples with $P_{\rm out} < 1000$ days. Table 4 hints that triples with less eccentric outer orbits or longer inner periods are aligned more frequently, although the differences are not statistically significant. No difference in alignment is found by splitting the sample around 1.3 $M_\odot$ mass.

The width of the cosine distribution in the aligned systems suggests mutual inclinations Φ within ∼20°. To quantify better, I simulated 10^4 triples where a 0.25 fraction has mutual inclinations Φ uniformly distributed in specified intervals, while the rest have random alignment. The lower panel of Figure 8 shows three representative simulated distributions of $|\cos i_{\rm out}|$. A uniform Φ distribution between 0° and 20° produces a sharp peak near zero that does not resemble the actual histogram, and a concentration of Φ around 39°predicted by D. Fabrycky & S. Tremaine (2007) is also excluded. A qualitative match to the observed histogram shape is found for Φ between 10° and 20°. However, these simulations do not account for the histogram broadening by measurement errors.

In the majority of misaligned compact triples, the precession of the inner pair should change the inclination and, consequently, the eclipse depth. However, typical precession periods are long (∼3 kyr for inner and outer periods of 1 and 1000 days), leaving detection of such effects for the future, except the few known examples.

4. DISCUSSION

4.1. *Theoretical Predictions*

To put this work in proper context, a broad outline of the formation of stellar hierarchies is in order. Figure 9 offers a visual guide to the following text; various processes contributing to the architecture of multiple systems are discussed in A. Tokovinin (2021b).

Stars form in groups: clusters, associations, and small aggregates. Nascent groups are highly structured, inheriting the spatial distribution of the molecular gas, and this reflects in the hierarchy of young multiple systems at large spatial scales (I. Joncour et al. 2017). Interactions between the stars are governed by the Newtonian dynamics of point masses (N-body). The decay of young stellar groups inevitably leaves some surviving bound wide triples. Their architecture bears imprints of the chaotic dynamics: the orbits are not aligned mutually, the inner orbits have the thermal eccentricity distribution $f(e) = 2e$, and the ratios of outer and inner separations are modest, not too far above the dynamical stability limit (J. M. O. Antognini & T. A. Thompson 2016). The properties of wide triples in the field match the N-body predictions (A. Tokovinin 2022; C. Shariat et al. 2025). However, they show signs of weak orbit alignment at outer separations below ∼100 au, where the dynamical effect of the gas becomes important.

Median separations of binaries are in the range of 10 to 100 au, so the architecture of typical stellar systems depends on the processes involving gas, such as core fragmentation, disk fragmentation, gas-assisted capture, and accretion (S. S. R. Offner et al. 2023). P. F. Rohde et al. (2021) explored numerically the collapse of isolated 1 $M_\odot$ cores of ∼3 kau initial radius; on average, they produce 3.1 stars per core. The mass ratios q of these low-mass binaries mostly exceed 0.6, and 43% are twins with $q > 0.95$; their separations are below 100 au. The outflows increase the fraction of twins by blocking gas supply from polar directions and enhancing infall from the equatorial plane, where most mass is accreted by the secondary component. Although some triples are dynamically unstable and decay, new systems form, so the fraction of hierarchies remains almost constant at 0.17±0.03 during the simulations. It is substantially higher than ∼0.05 for stars of 0.5 $M_\odot$ in Figure 1 of S. S. R. Offner et al. (2023). The relatively large percentage of hierarchies produced in the simulations of P. F. Rohde et al. (2021) could be related to the core rotation. Unfortunately, their paper does not explore the orbit alignment in triples. M. R. Bate (2014) presents the multiplicity statistics resulting from his simulations of cluster collapse. The orbits of 31 triples are relatively well aligned with $\langle\Phi\rangle = 39°$. A dependence of the alignment on the outer separation and period ratio is found (see their Figure 20), matching the observed trends.

The accretion of gas accompanied by inward migration is the generally accepted process creating close binaries, including inner subsystems in triples. The partial alignment of triples with outer separations below 100 au is presumably caused by the accretion of gas with a relatively constant angular momentum inherited

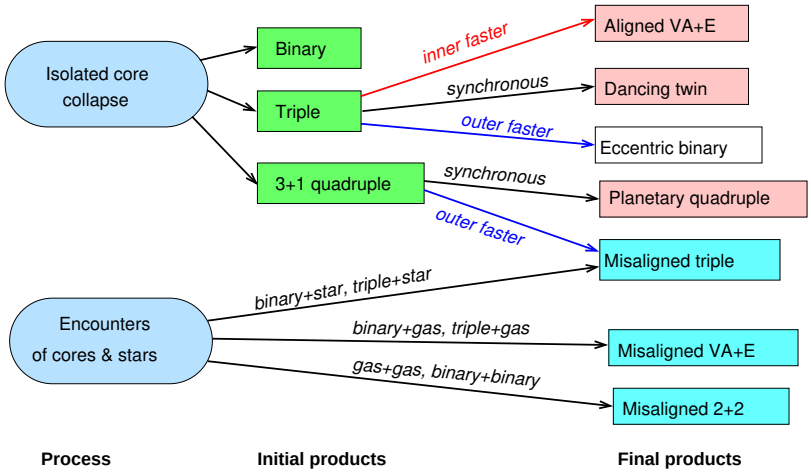

Figure 9. Formation and early evolution of hierarchical systems (section 4.1). VA+E stands for compact triples with eclipsing inner pairs.

from the parent core; it naturally extends to the alignment between binary orbits and stellar rotation axes (M. R. Bate 2014). The aligned gas is accreted preferentially by the secondary component, increasing the mass ratio and producing twins (A. Tokovinin & M. Moe 2020). Many twins are found in the inner subsystems of hierarchies, and double twins where both inner and outer mass ratios are close to one are also typical for low-mass hierarchies with moderate outer separations (A. Tokovinin 2018c), including in this sample. Such hierarchies, "dancing twins", are also approximately aligned and have moderately eccentric orbits. A related class are the aligned 3+1 "planetary" quadruples such as HD 91962 (A. Tokovinin et al. 2015) or the compact (periods 2.9 days, 59 days, and 3.9 years) low-mass quadruple HIP 41431 (T. Borkovits et al. 2019).

Although approximately aligned triples and 3+1 quadruples can be linked to the products of isolated core collapse, theoretical predictions of their properties are still vague. If the infalling gas is accreted mostly by the outer component of a triple and it migrates faster than the inner binary, the system may become dynamically unstable and disrupt, leaving behind an eccentric binary (or a misaligned triple after decay of a quadruple). On the other hand, the migration in the inner and outer subsystems can be somehow synchronized at the period ratio on the order of 20, when the subsystems already interact mutually but the triple remains stable; such period ratios are typical for dancing twins and planetary-type quadruples. The existence of compact (e.g. eclipsing and triply eclipsing) and aligned hierarchies (T. Borkovits et al. 2016) indicates that migration can shrink inner orbits very efficiently without destroying the system. The three possible types of accreting triple evolution (inner faster, synchronized, and outer faster) are coded by the red, black, and blue lines, respectively, in Figure 9.

Interactions of the products of core fragmenation with neighboring stars and gas (e.g. between two fragments of the filament falling on to the common center of mass) can alter the final stellar systems or trigger the collapse. A. P. Whitworth (2001) proposed that collisions between two cores can spawn relatively wide 2+2 quadruples. A triple formed by an isolated core collapse can be disrupted by another approaching star; an encounter between two binaries can produce a misaligned triple. A misaligned gas falling on to a triple can be captured preferentially by the inner subsystem, causing its fast migration and producing a triple with misaligned tight inner pair. This could be a dominant channel of close binary formation within triples. Encounters could potentially explain the empirical correlation between close binaries and hierarchical multiplicity and the correlated occurrence of subsystems in both components of wide binaries inferred from the relatively high frequency of 2+2 quadruples in the field (A. Tokovinin 2014). However, theoretical studies of these mechanisms yielding quantitative predictions are needed. Misaligned gas structures are directly observed in young hierarchies such as the quadruple HD 98800 (S. Zúñiga-Fernández et al. 2021) and the triple GW Ori, a member of our sample (S. Kraus et al. 2020).

The multiplicity is a strong function of mass (G. Duchêne & A. Kraus 2013; S. S. R. Offner et al. 2023). Formation of massive stars and stellar systems requires mass assembly from a large volume (P. C. Clark & A. P. Whitworth 2021; P. Hennebelle & M. Y. Grudić 2024). Their properties are shaped by interactions with stellar neighbors and gas outside the original cores to a larger extent,

compared to low-mass hierarchies. Qualitatively, the dependence of the architecture of stellar systems on their mass and size agrees with the expected role of encounters. The observed trends can be interpreted as a mixture in varying proportion between approximately aligned pristine hierarchies and misaligned products of their interaction with the environment.

4.2. *Inferences from This Study*

The sample of resolved triples with outer separation below ∼300 au reveals clear trends in the mutual orbit alignment and mass ratios, in agreement with previous studies. These trends can be matched qualitatively to the mechanisms of triple-star formation outlined above.

1. Alignment decreases with increasing outer separation and vanishes at $s > 300$ au because wider triples are shaped by N-body dynamics, while gas dynamics is relevant at spatial scales comparable to the size of accretion disks and smaller. The influence of gas accretion is also demonstrated by the substantial fraction of inner twins and by moderate inner eccentricities in aligned triples, which were presumably damped by dissipation in a disk. Most triples with eccentric inner orbits ($e_{\rm in} > 0.7$) are not aligned.

2. The alignment decreases with increasing ratio of outer and inner separations or periods, with decreasing inner mass ratio, and with increasing mass. These trends can be explained by the accretion of misaligned gas unrelated to the original core. The average mutual inclination in the full sample is 40°, but in a subset of 38 triples with primary components less massive than 1 $M_\odot$ and outer separations below 50 au it is 10°.

3. Triple systems in non-hierarchical configurations ("trapezia") are found not only at wide separations, but also at orbit sizes of ∼10 au. These field triples are close to the dynamical stability limit. Their existence suggests that migration could destabilize and disrupt relatively compact triples, and that low-mass trapezia in the field (Figure 1) are their surviving subset.

4. A substantial fraction of triple systems in this sample (46 out of 278) have additional distant companions at separations of $10^3 - 10^4$ au. This indicates that they were formed in sparse environments, rather than in clusters. Their architecture therefore is relevant to fragmentation of isolated cores.

5. Inner orbits in 63 2+2 quadruples with outer separations from 100 to 10^4 au are not mutually aligned.

6. Only 22% of triples with known outer orbits and inner eclipising subsystems are mutually aligned within ∼20°, the rest are aligned randomly. The fraction of aligned triples is larger for outer periods under 1000 days.

This study explores the separation regime from a few to 300 au, on the order of median separation of low-mass binaries. Its results are complemented by the statistics at larger separations provided by C. Shariat et al. (2025) and A. Tokovinin (2022), showing the transition between close (gas-dominated) and wide (N-body) regimes. Apparently, collapse of isolated cores typically produces low-mass stars and well-organized planar hierarchies. At still smaller separations, we expect an even stronger imprint of the gas accretion, leading to aligned orbits. The compact eclipsing triples have a preferentially flat architecture and are often aligned within a few degrees (T. Borkovits et al. 2016; T. Borkovits 2022); for this reason, many such hierarchies are triply eclipsing. However, the properties of eclipsing subsystems explored in section 3.5 are at odds with this view, showing that in 3/4 of such hierarchies, even in compact ones, the relative orbit alignment is random. The division of eclipsing triples in two groups (aligned and random) and the outliers contradicting the general trends suggest that hierarchical systems were formed via different processes and their combinations (Figure 9).

4.3. *Future Work*

The complexity of triple-star formation reflected in their statistics tells us that considering these objects without distinction in separation, mass, etc., as a single population, hides the trends and is not very informative. Early statistical studies did not allow such distinction owing to the small samples. Ground-based monitoring and space surveys will enlarge the samples to clarify known trends and to find new ones. The SOAR program on multiple stars illustrates the need of a long time coverage combined with high angular resolution for revealing the architecture of stellar hierarchies. Its continuation and extension to the northern sky would be promising.

The diversity of initial conditions and processes involved in the star formation stand on the way of predicting statistical properties of stellar systems. While a general understanding is reached, and the simulations match the observed statistics qualitatively, much work remains to be done. Large-scale hydrodynamic sim-

ulations (M. R. Bate 2014) are expensive and have a low statistical yield. Targeted simulations on smaller scales sampling a range of physical parameters, initial conditions, and random realizations, like those of P. F. Rohde et al. (2021), is a promising way forward. The role of accretion in shaping the masses and orbital architecture of binaries and triples is not yet fully explored, despite several studies. For example, the synopsis of hydrodynamic simulations of accreting binaries by R. Valli et al. (2024) treats only the planar two-dimensional case, while in reality the misalignment of gas is essential, and the problem is intrinsically three-dimensional (J. L. Smallwood et al. 2025).

ACKNOWLEDGMENTS

The research was funded by the NSF's NOIRLab. Comments by the anonymous Referee helped to improve the clarity of presentation. This work used the SIMBAD service operated by Centre des Données Stellaires (Strasbourg, France), bibliographic references from the Astrophysics Data System maintained by SAO/NASA, and the Washington Double Star Catalog maintained at USNO. This work has made use of data from the European Space Agency (ESA) mission Gaia (https://www.cosmos.esa.int/gaia), processed by the Gaia Data Processing and Analysis Consortium (DPAC, https://www.cosmos.esa.int/web/gaia/dpac/consortium). Funding for the DPAC has been provided by national institutions, in particular the institutions participating in the Gaia Multilateral Agreement.

Facility: SOAR, Gaia

REFERENCES

Albrecht, S. H., Dawson, R. I., & Winn, J. N. 2022, PASP, 134, 082001, doi: 10.1088/1538-3873/ac6c09

Antognini, J. M. O., & Thompson, T. A. 2016, MNRAS, 456, 4219, doi: 10.1093/mnras/stv2938

Bate, M. R. 2014, MNRAS, 442, 285, doi: 10.1093/mnras/stu795

Borkovits, T. 2022, Galaxies, 10, 9, doi: 10.3390/galaxies10010009

Borkovits, T., Hajdu, T., Sztakovics, J., et al. 2016, MNRAS, 455, 4136, doi: 10.1093/mnras/stv2530

Borkovits, T., Sperauskas, J., Tokovinin, A., et al. 2019, MNRAS, 487, 4631, doi: 10.1093/mnras/stz1510

Bouy, H., Martín, E. L., Brandner, W., & Bouvier, J. 2005, AJ, 129, 511, doi: 10.1086/426559

Christian, S., Vanderburg, A., Becker, J., et al. 2025, AJ, 169, 308, doi: 10.3847/1538-3881/adc933

Clark, C. A., van Belle, G. T., Horch, E. P., et al. 2024, AJ, 167, 174, doi: 10.3847/1538-3881/ad267d

Clark, P. C., & Whitworth, A. P. 2021, MNRAS, 500, 1697, doi: 10.1093/mnras/staa3176

Czavalinga, D. R., Mitnyan, T., Rappaport, S. A., et al. 2023, A&A, 670, A75, doi: 10.1051/0004-6361/202245300

Duchêne, G., & Kraus, A. 2013, ARA&A, 51, 269, doi: 10.1146/annurev-astro-081710-102602

Dupuy, T. J., Kraus, A. L., Kratter, K. M., et al. 2022, MNRAS, 512, 648, doi: 10.1093/mnras/stac306

El-Badry, K., Rix, H.-W., & Heintz, T. M. 2021, MNRAS, 506, 2269, doi: 10.1093/mnras/stab323

Fabrycky, D., & Tremaine, S. 2007, ApJ, 669, 1298, doi: 10.1086/521702

Gaia Collaboration, Brown, A. G. A., Vallenari, A., et al. 2021, A&A, 649, A1, doi: 10.1051/0004-6361/202039657

Gaia Collaboration, Brown, A. G. A., Vallenari, A., et al. 2016, A&A, 595, A2, doi: 10.1051/0004-6361/201629512

Hartkopf, W. I., Mason, B. D., & Worley, C. E. 2001, AJ, 122, 3472, doi: 10.1086/323921

Hennebelle, P., & Grudić, M. Y. 2024, ARA&A, 62, 63, doi: 10.1146/annurev-astro-052622-031748

Janson, M., Bergfors, C., Brandner, W., et al. 2014, ApJS, 214, 17, doi: 10.1088/0067-0049/214/2/17

Joncour, I., Duchêne, G., & Moraux, E. 2017, A&A, 599, A14, doi: 10.1051/0004-6361/201629398

Kraus, S., Kreplin, A., Young, A. K., et al. 2020, Science, 369, 1233, doi: 10.1126/science.aba4633

Lane, B. F., Muterspaugh, M. W., Fekel, F. C., et al. 2007, ApJ, 669, 1209, doi: 10.1086/520877

Leinert, C., Henry, T., Glindemann, A., & McCarthy, Jr., D. W. 1997, A&A, 325, 159

Makarov, V. V. 2025, AJ, 170, 138, doi: 10.3847/1538-3881/adec79

Marcussen, M. L., & Albrecht, S. H. 2022, ApJ, 933, 227, doi: 10.3847/1538-4357/ac75c2

Mardling, R. A., & Aarseth, S. J. 2001, MNRAS, 321, 398, doi: 10.1046/j.1365-8711.2001.03974.x

Mason, B. D., Wycoff, G. L., Hartkopf, W. I., Douglass, G. G., & Worley, C. E. 2001, AJ, 122, 3466, doi: 10.1086/323920

Offner, S. S. R., Moe, M., Kratter, K. M., et al. 2023, in Astronomical Society of the Pacific Conference Series, Vol. 534, Protostars and Planets VII, ed. S. Inutsuka, Y. Aikawa, T. Muto, K. Tomida, & M. Tamura, 275, doi: 10.48550/arXiv.2203.10066

Pecaut, M. J., & Mamajek, E. E. 2013, ApJS, 208, 9, doi: 10.1088/0067-0049/208/1/9

Rohde, P. F., Walch, S., Clarke, S. D., et al. 2021, MNRAS, 500, 3594, doi: 10.1093/mnras/staa2926

Shariat, C., El-Badry, K., & Naoz, S. 2025, PASP, 137, 094201, doi: 10.1088/1538-3873/adfb30

Smallwood, J. L., Li, Y.-P., Deng, H., & Franchini, A. 2025, MNRAS, 536, 3431, doi: 10.1093/mnras/stae2768

Sterzik, M. F., & Tokovinin, A. A. 2002, A&A, 384, 1030, doi: 10.1051/0004-6361:20020105

Tokovinin, A. 2014, AJ, 147, 87, doi: 10.1088/0004-6256/147/4/87

Tokovinin, A. 2017, ApJ, 844, 103, doi: 10.3847/1538-4357/aa7746

Tokovinin, A. 2018a, ApJS, 235, 6, doi: 10.3847/1538-4365/aaa1a5

Tokovinin, A. 2018b, PASP, 130, 035002, doi: 10.1088/1538-3873/aaa7d9

Tokovinin, A. 2018c, AJ, 155, 160, doi: 10.3847/1538-3881/aab102

Tokovinin, A. 2021a, AJ, 161, 144, doi: 10.3847/1538-3881/abda42

Tokovinin, A. 2021b, Universe, 7, 352, doi: 10.3390/universe7090352

Tokovinin, A. 2022, ApJ, 926, 1, doi: 10.3847/1538-4357/ac4584

Tokovinin, A. 2023a, AJ, 165, 165, doi: 10.3847/1538-3881/acbf32

Tokovinin, A. 2023b, AJ, 165, 180, doi: 10.3847/1538-3881/acc464

Tokovinin, A. 2025a, AJ, 169, 124, doi: 10.3847/1538-3881/ada3c6

Tokovinin, A. 2025b, AJ, 170, 143, doi: 10.3847/1538-3881/adee23

Tokovinin, A. 2025c, Contributions of the Astronomical Observatory Skalnate Pleso, 55, 243, doi: 10.31577/caosp.2025.55.3.243

Tokovinin, A., & Briceño, C. 2020, AJ, 159, 15, doi: 10.3847/1538-3881/ab5525

Tokovinin, A., & Kiyaeva, O. 2016, MNRAS, 456, 2070, doi: 10.1093/mnras/stv2825

Tokovinin, A., & Latham, D. W. 2017, ApJ, 838, 54, doi: 10.3847/1538-4357/aa6331

Tokovinin, A., & Latham, D. W. 2020, AJ, 160, 251, doi: 10.3847/1538-3881/abbad4

Tokovinin, A., Latham, D. W., & Mason, B. D. 2015, AJ, 149, 195, doi: 10.1088/0004-6256/149/6/195

Tokovinin, A., Mason, B. D., & Hartkopf, W. I. 2010, AJ, 139, 743, doi: 10.1088/0004-6256/139/2/743

Tokovinin, A., Mason, B. D., Mendez, R. A., & Costa, E. 2024, AJ, 168, 28, doi: 10.3847/1538-3881/ad4d56

Tokovinin, A., & Moe, M. 2020, MNRAS, 491, 5158, doi: 10.1093/mnras/stz3299

Tokovinin, A., Petr-Gotzens, M. G., & Briceño, C. 2020, AJ, 160, 268, doi: 10.3847/1538-3881/abc2d6

Torres, G., Schaefer, G. H., Monnier, J. D., et al. 2022, ApJ, 941, 8, doi: 10.3847/1538-4357/ac9d8d

Valli, R., Tiede, C., Vigna-Gómez, A., et al. 2024, A&A, 688, A128, doi: 10.1051/0004-6361/202449421

Whitworth, A. P. 2001, in The Formation of Binary Stars, ed. H. Zinnecker & R. Mathieu, Vol. 200, 33

Winters, J. G., Henry, T. J., Jao, W.-C., et al. 2019, AJ, 157, 216, doi: 10.3847/1538-3881/ab05dc

Worley, C. E. 1967, in On the Evolution of Double Stars, ed. J. Dommanget, Vol. 17, 221

Xia, F., Fu, Y., & Wang, X. 2019, ApJ, 882, 147, doi: 10.3847/1538-4357/ab32de

Zúñiga-Fernández, S., Olofsson, J., Bayo, A., et al. 2021, A&A, 655, A15, doi: 10.1051/0004-6361/202141985